Journal of Superconductivity and Novel Magnetism (2020) 33:775–781
https://doi.org/10.1007/s10948-019-05258-7

ORIGINAL PAPER

Microstructure Regulation and Coercivity Improvement in the Dy_2O_3/WS_2 Co-doped Nd-Fe-B–Sintered Magnets

Fang Yang[1] · Qian Qin[1] · Shengzeng Lin[1] · Haixia Sun[1] · Yanli Sui[2] · Zhimeng Guo[1] · Alex A. Volinsky[3]

Received: 12 June 2019 / Accepted: 9 August 2019 / Published online: 17 August 2019

Abstract

In this study, the effects of Dy_2O_3/WS_2 co-doping on magnetic properties and microstructure of Nd-Fe-B–sintered magnets were investigated. With WS_2 addition, microstructure regulation and coercivity improvement were achieved in the Dy-containing magnets. The optimal magnetic performance was obtained in the 2 wt% Dy_2O_3/0.4 wt% WS_2 co-doped magnets. The coercivity, remanence, and maximum energy product were 1727.1 kA/m, 1.211 T, and 286.5 kJ/m^3, respectively. The coercivity was 10.5% higher than the WS_2-free magnets, while there was no obvious change in the remanence and the maximum energy product. Relatively clear grain boundary phases were observed with smaller grain size. The average grain size of the co-doped magnets was 6.4 μm, which was about 1.6 μm smaller than the WS_2-free magnets. More uniform Dy distribution was also obtained with the Nd_2O_2S phase formation. Besides, the W element likely precipitated at the grain boundaries.

Keywords Nd-Fe-B–sintered magnets · WS_2 · Co-doping · Microstructure · Coercivity

1 Introduction

Due to their excellent energy products, Nd-Fe-B–sintered magnets are widely used in the new energy field, including hybrid electric vehicles, wind turbines, and wind power generators [1, 2]. Moreover, there is an increasing demand for their further applications at elevated temperatures (above 200 °C), which requires that the room temperature coercivity should be higher than 1600 kA/m [3, 4]. Although the remanence and the maximum energy product of the Nd-Fe-B–sintered magnets are close to their theoretical values, the coercivity only reaches ~ 30% of the anisotropy field of the $Nd_2Fe_{14}B$ phase [5]. Generally, rare earth Dy element is introduced into the magnets to significantly enhance the coercivity due to the higher anisotropy field of the $Dy_2Fe_{14}B$ phase. In such a case, the ideal scenario is when Dy atoms only precipitate in the outer regions of the $Nd_2Fe_{14}B$ phase forming a Dy-rich shell [6, 7]. Due to the remanence decrease and resource scarcity, along with high cost, there is a trend to reduce the usage of the Dy element without sacrificing the coercivity.

Among all technologies of introducing the Dy element into magnets, the methods based on grain boundary diffusion have attracted much attention, where the Dy atoms only diffuse into the outer region of the 2:14:1 phase. As a drawback, it is only suitable for the magnets with a limited thickness [8, 9]. Without the restriction on the size of the magnets, multiple efforts on the Dy compounds powder doping prior to sintering have been reported [10, 11]. Thereinto, Dy_2O_3 is the most commercial additive for the Nd-Fe-B–sintered magnets. However, inhomogeneous Dy distribution has been found in the magnets with Dy_2O_3 addition [12–14]. Most of the Dy atoms are enriched in the triple junction regions of the Nd-rich phases due to their higher affinity to O atoms [15]. To solve this problem, Dy_2S_3 instead of Dy_2O_3 has been introduced into the magnets [16]. Dy saving and coercivity improvement have been achieved with the formation of the Nd-O-S phase. Dy atoms have been found to avoid the Nd-O-S phase, resulting in more available Dy atoms diffusing into the main phases [16, 17]. Besides, in our previous studies, the sulfur element would significantly decrease the melting temperature, thus optimizing the

✉ Fang Yang
yangfang@ustb.edu.cn

[1] Institute for Advanced Materials and Technology, University of Science and Technology Beijing, Beijing 100083, China

[2] State Key Laboratory for Advanced Metals and Materials, University of Science and Technology Beijing, Beijing 100083, China

[3] Department of Mechanical Engineering, University of South Florida, Tampa, FL 33620, USA

microstructure [18, 19]. Furthermore, in Bae et al.'s study, WS_2 has been proven to effectively inhibit grain growth. The interactions between W and Al elements have been systematically studied [20]. However, the S effect in WS_2-containing magnets has not been studied.

In this study, we investigated the effects of Dy_2O_3/WS_2 co-doping on the microstructure and magnetic performance of the Nd-Fe-B–sintered magnets. The relationships between W, S, and Dy elements were evaluated. Besides, the microstructure changes, element distribution and phase transformations were systematically discussed.

2 Experimental Procedure

2.1 Preparation

The Nd-Fe-B powder (3–5 μm, purchased from the Tianjin Sanhuan Lucky New Materials Inc.), the Dy_2O_3 powder (1–3 μm, purchased from the China Grirem Advanced Materials Co., Ltd), and the WS_2 powder (1–3 μm, Sinopharm Chemical Reagent Co., Ltd) were chosen as the raw materials. First, the Nd-Fe-B powders of 32.5Re (Re-Nd, Pr, Gd)-bal. Fe-1.0B-1.54M (wt%, M-Al, Co, Cr, Cu) were mixed with Dy_2O_3 (2 wt%) and WS_2 (0, 0.2, 0.4, and 0.6 wt.%) powders by the V-type mixer for 2 h. Then, the mixed powders were compacted in 1352 kA/m magnetic field. Subsequently, the green compacts were vacuum-sintered at 1045 °C for 6 h with a heating rate of 4 °C/min. After sintering, the magnets were furnace-cooled to 930 °C for 2 h followed by argon-cooling to room temperature. Finally, the annealing treatment was carried out at 510 °C for 5 h.

2.2 Tests and Characterization

Four samples were prepared for each test to confirm repeatability. The sintered density was measured according to the Archimedes' method. The room temperature magnetic performance was determined by a magnetic measurement device (NIM-200C). The microstructure observations were carried out using field emission scanning microscopy (FESEM, Zeiss Supra55). The grain size distribution was analyzed by an image analyzer (UTHSCSA Image Tool). Elemental distribution was conducted by electron probe microanalysis (EPMA, JEOL, JXA-8230) combined with energy dispersive spectroscopy (EDS). Phase characterization was performed using transmission electron microscopy (TEM, Tecnai G2 F30 S-TWIN) combined with selected area electron diffraction (SAED). An ion milling system was employed to prepare a thin foil sample for TEM analysis.

3 Results and Discussion

After sintering, all magnets were nearly completely dense, as shown in Table 1. The density was above 7.55 g/cm^3. Although the volume percent of the $Nd_2Fe_{14}B$ phase decreased with Dy_2O_3 and WS_2 addition, the decrease of sintered density was not obvious. The density of Dy_2O_3 was 7.81 g/cm^3, while that of WS_2 was 7.5 g/cm^3, which were close to the density of the Nd-Fe-B magnets. This was the reason why the decrease in density was not obvious with the Dy_2O_3 and WS_2 co-doping. Figures 1 and 2 present the magnetic performance of the co-doped magnets. For the magnets containing 2 wt% Dy_2O_3, the corresponding coercivity (H_{cj}), remanence (B_r), and maximum energy product $(BH)_{max}$ were 1.219 T, 1563.2 kA/m, and 288.2 kJ/m^3, respectively. With increasing WS_2 content, the H_{cj} increased before decreasing, while B_r and $(BH)_{max}$ continuously decreased. The maximum H_{cj} value was obtained in the 2 wt% Dy_2O_3/0.4 wt% WS_2 co-doped magnets. Correspondingly, the H_{cj} value was 1727.1 kA/m, which was 10.5% higher than the WS_2-free magnets. The values of B_r and $(BH)_{max}$ were 1.211 T and 286.5 kJ/m^3, respectively. It is worth noting that there was no obvious decrease in B_r and $(BH)_{max}$ with the 0.4 wt% WS_2 addition. With excess WS_2 addition, the H_{cj} reduced. Therefore, the optimal WS_2 content for the co-doped magnets was 0.4 wt%.

The coercivity change was closely related to the microstructure. Therefore, the microstructure and grain size distribution were characterized, as shown in Fig. 3. Typical microstructure of Nd-Fe-B–sintered magnets was observed, which mainly consisted of the $Nd_2Fe_{14}B$ phase and the Nd-rich phase. The dark region is the main phase, while the bright region is the Nd-rich phase. As shown in Fig. 3(a), no obvious grain boundary phase (GBP) was observed. In theory, thin and continuous GBP should be distributed along the $Nd_2Fe_{14}B$ phase to weaken the magnetic exchange interaction between adjacent grains. The average grain size of the WS_2-free magnets was about 8 μm. In contrast, thin and obvious GBP was obtained in the co-doped magnets with 0.4 wt% WS_2 addition, as shown in Fig. 3(b). With WS_2 addition, grain refinement and more uniform grain size distribution were achieved. The average grain size of the co-doped magnets was about 6.44 μm, which was approximately 1.6 μm smaller than the WS_2-free magnets. Therefore, the coercivity improvement of the co-doped magnets was attributed to grain refinement and GBP optimization. Refractory metal (RM), such as W, was an effective additive to inhibit the grain growth by grain boundary pinning [21]. As for the S element, it also helped to refine the grain due to the decrease of melting temperature of the Nd-rich phase [18, 19].

To evaluate the relationships between W, S, and Dy atoms, the elemental distribution analysis was carried out. As shown in Fig. 4, the Nd-rich phases mainly consisted of Nd and O

Table 1 Density of the co-doped magnets with different WS_2 contents

WS_2 content (wt%)	0	0.2	0.4	0.6
Density (g/cm^3)	7.59 ± 0.01	7.59 ± 0.01.	7.58 ± 0.01.	7.56 ± 0.01.

elements. The distribution of the Dy element was nonuniform, just as the marked white circle. Part of the Dy atoms were enriched in the Nd-rich phases at the triple junction regions due to their high affinity to O atoms. This result was consistent with the literature [12–14]. Compared with the WS_2-free magnets, the distribution of the Dy element in the co-doped magnets was more uniform, as shown in Fig. 5. No Dy clusters were observed in the triple junction regions. The Nd-rich phases were mainly composed of Nd, O, and S elements. It can be inferred that the S-rich phase should be neodymium (oxy)sulfide. As reported in the studies [16, 17], with the S element introduction, the Nd_2O_2S phase was formed instead of Nd_xO_y phase, and Dy atoms were excluded by the Nd_2O_2S phase, resulting in more Dy atoms diffusing into the $Nd_2Fe_{14}B$ phase and coercivity improvement. It was worth noting that although W element was also introduced into the magnets, the distribution of W was not obvious without W-rich phase being detected.

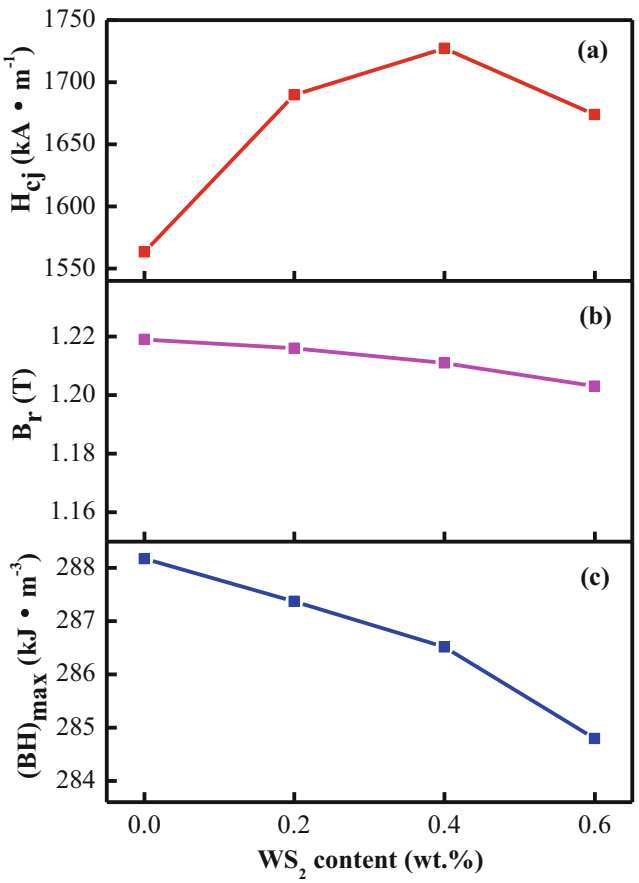

Fig. 1 The changes of **a** H_{cj}, **b** B_r, and **c** $(BH)_{max}$ for Dy_2O_3/WS_2 co-doped magnets with different WS_2 contents

Correspondingly, the EPMA-EDS line scans were performed to analyze the change of elemental distribution in different phases, as shown in Fig. 6. In the WS_2-free magnets, Nd, O, and Dy elements were detected in the Nd-rich phase, and the result was consistent with Fig. 4. In contrast, no obvious peaks of Dy element were observed in the Nd-rich phase of the co-doped magnets, as shown in Fig. 6(b). Interestingly, the S element was found in the Nd-rich phase instead of the Dy element. However, the distribution of S element was not uniform. It can be inferred that the Nd-rich phases at the triple junction regions were mainly composed of the Nd-O and Nd-O-S phases in the co-doped magnets. It was worth noting that there was one peak of W element, although the peak was not obvious. To further confirm the existence of the W element, the marked rectangle was magnified, shown as the purple EDS pattern. One peak of the W element was observed at the grain boundary. Therefore, the W element potentially precipitated at the grain boundary.

The phases' identification was carried out, as shown in Fig. 7. According to EDS analysis, region "A" was corresponding to the S-rich phase, which was enriched in the triple junction regions. Two sets of SAED patterns of the region "A" are presented in Figs. 7(b, c). The zone axis in Fig. 7(b) was corresponding to $[\bar{2}11]$, while in Fig. 7(c) it was analyzed as [100]. In terms of the SAED analysis, the S-rich phase was identified as hexagonal Nd_2O_2S phase with lattice parameters a = 0.395 nm, c = 0.679 nm. The HRTEM image and corresponding FFT image in Fig. 7(f) were characterized to further demonstrate the crystal structure of the S-rich phase. The obvious interface was observed, which was corresponding to the

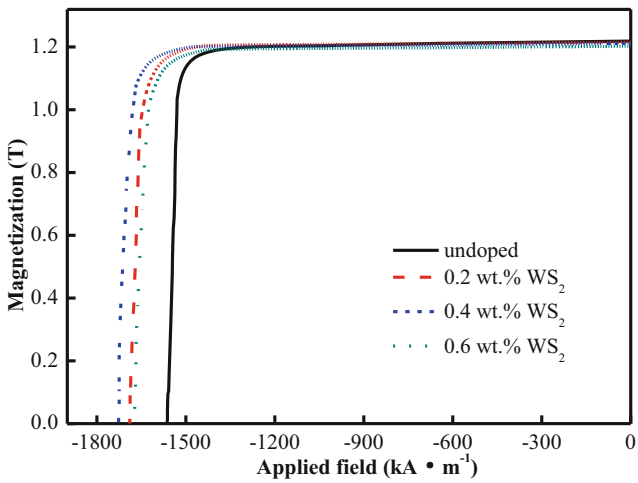

Fig. 2 The corresponding demagnetization curves of Dy_2O_3/WS_2 co-doped magnets

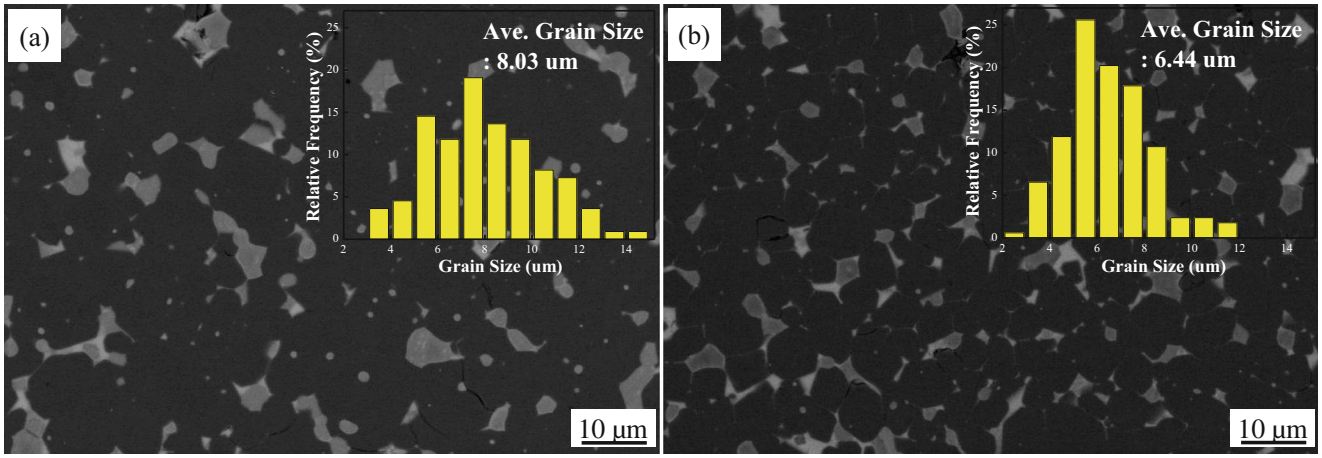

Fig. 3 Microstructure and grain size distribution of **a** 2 wt% Dy_2O_3-doped and **b** 2 wt% Dy_2O_3/0.4 wt% WS_2 co-doped magnets

grain boundary phase. It has been reported that the W element was found at the grain boundary phase-forming WFeB phase [20, 21]. Fine WFeB phase was effective to inhibit grain growth under the action of grain boundary pinning. However, there was no any W-rich phase found in the Dy_2O_3/WS_2 co-doped magnets by using TEM. In all regions, including the Nd-rich phase, the main phase, and the grain boundary phase, no such phase was detected. It might be related to the limited regions checked by the TEM analysis. Combined with the EPMA-EDS analysis in Fig. 6(b) and the reported studies [20, 21], it can be speculated that the W-rich phase precipitated at the grain boundary was the WFeB phase.

Therefore, the WS_2 addition can significantly increase the coercivity of the Dy-containing Nd-Fe-B–sintered magnets.

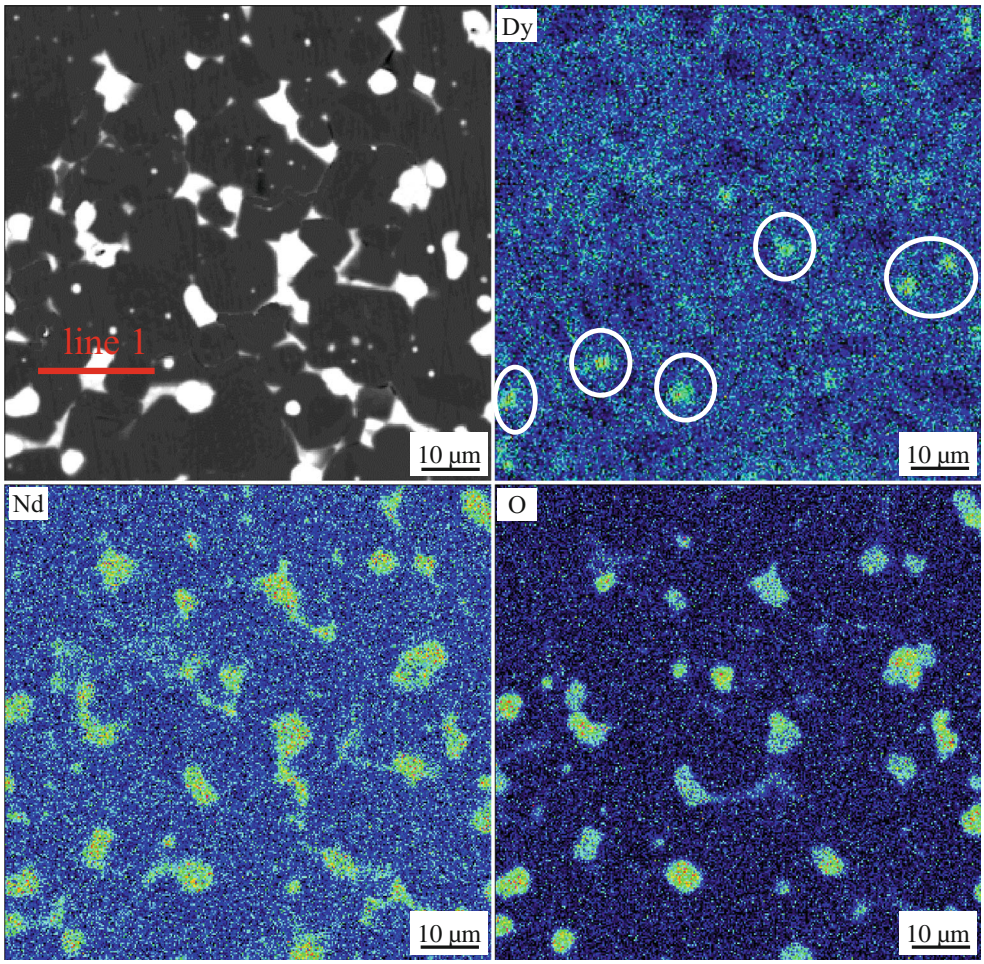

Fig. 4 Dy, Nd, and O elements distribution of WS_2-free magnets

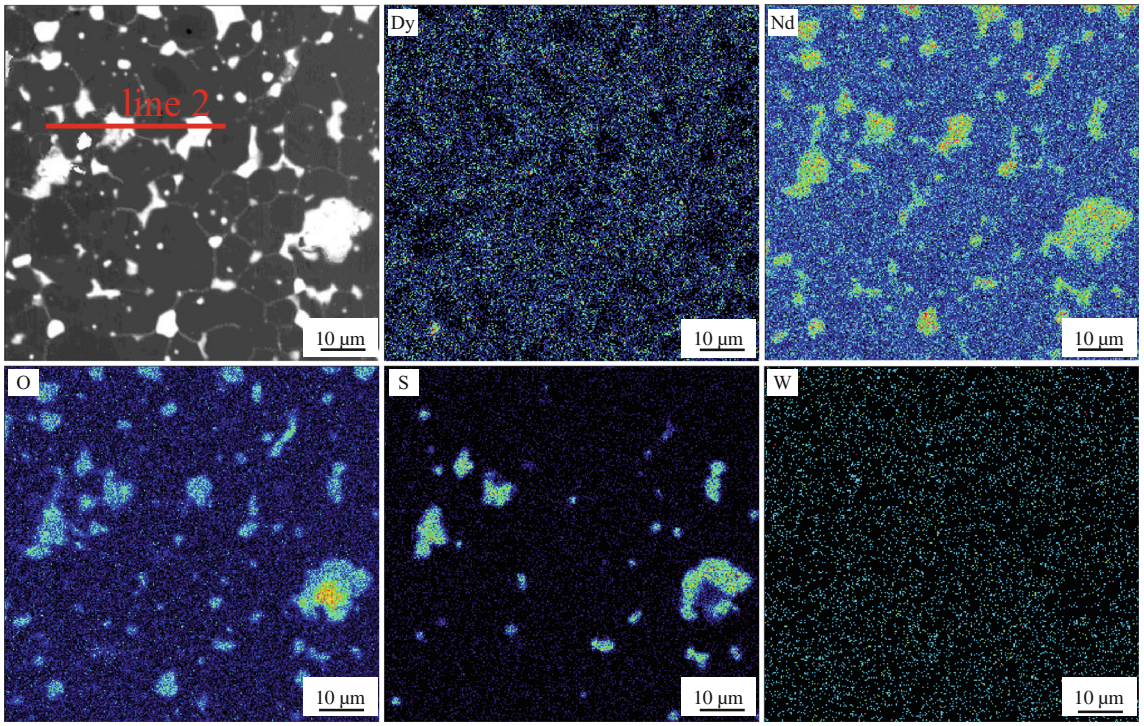

Fig. 5 Dy, Nd, O, S, and W elements distribution of 0.4 wt% WS_2 containing magnets

First, with the W introduction, W element would react with Fe and B elements to form fine WFeB phase at the grain boundary [20, 21]. As a result, the grain growth was inhibited. Then, S addition was known to decrease the melting point of the Nd-rich eutectic phase, thus also resulting in the grain refinement and GBP optimization. Combined with the above-mentioned factors, the average grain size of Dy_2O_3/WS_2 co-doped magnets was significantly decreased from 8 to 6.4 μm compared with the WS_2-free magnets. Besides, the distribution of the Dy element became more uniform due to the existence of the Nd_2O_2S phase. It has been reported that Dy atoms avoided the neodymium (oxy)sulfide phases [16]. This was why more available Dy atoms diffused into the 2:14:1 phase. Overall, the coercivity improvement of the co-doped magnets was attributed to grain refinement, grain boundary modification, and the optimization of Dy distribution. The optimal WS_2 content was 0.4 wt% in the co-doped magnets. Correspondingly, coercivity improvement of 10.5% was achieved with a slight decrease of the remanence and maximum energy product. With excessive WS_2 addition, the coercivity began to decrease. In such a case, although there was no big difference between the sintered density of the magnets, the volume percent of the main phase decreased accordingly. More Fe and B atoms were consumed from the main phase to form the WFeB phase. Moreover, as reported in the literature [20], large WFeB precipitates were observed in the magnets with 0.6 wt% WS_2 addition. These two reasons might give rise to the lower coercivity.

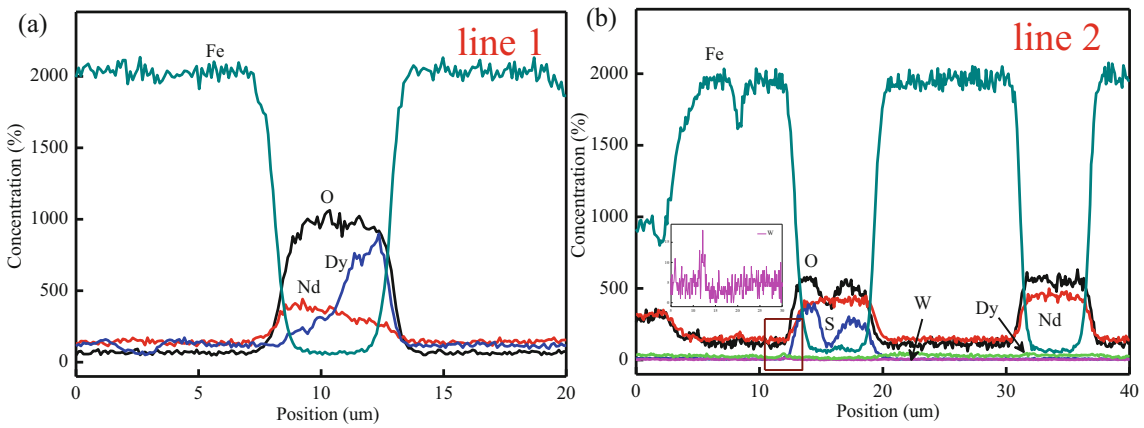

Fig. 6 EPMA-EDS line scan patterns taken from the red arrows in **a** Fig. 4 and **b** Fig. 5

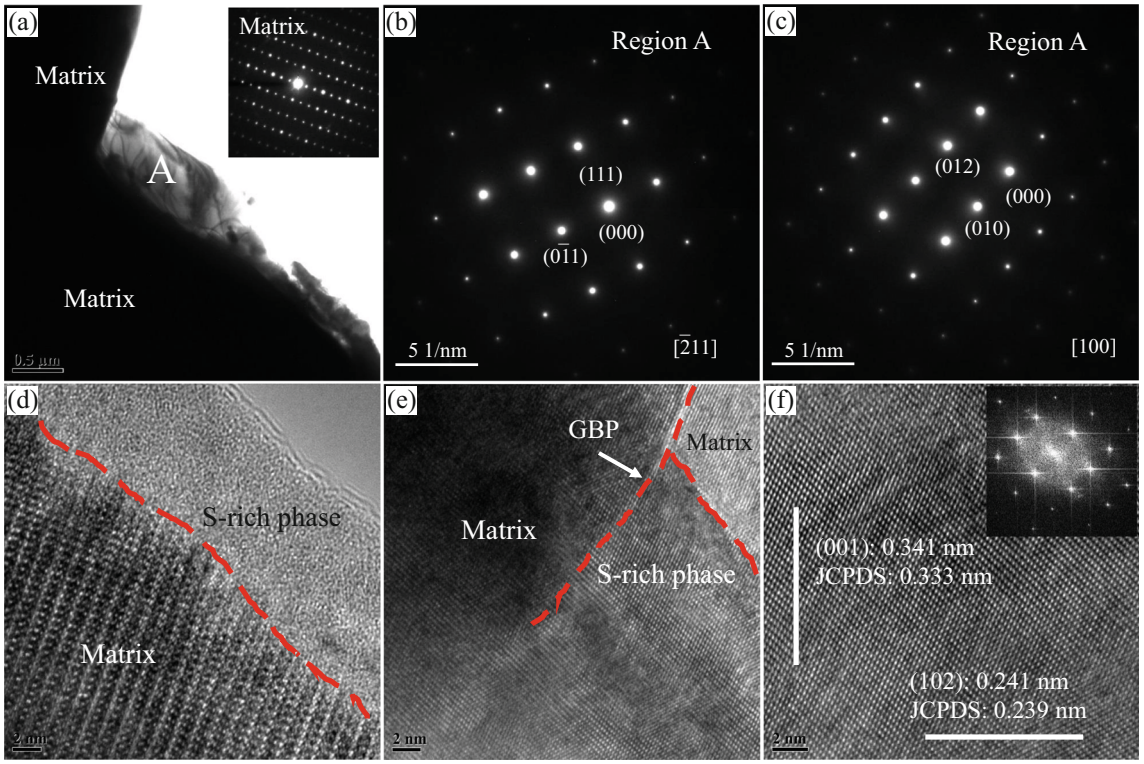

Fig. 7 **a** TEM image of 2 wt% Dy_2O_3/0.4 wt% WS_2 co-doped magnets, **b**, **c** SAED patterns of region A, and corresponding HRTEM images of **d**, **e** grain boundaries, and **f** S-rich phase

4 Conclusions

In summary, the magnetic performance, microstructure, elemental distribution, and phase transformations of Dy_2O_3/WS_2 co-doped Nd-Fe-B–sintered magnets were studied. In the 2 wt% Dy_2O_3-doped magnets, no clear and continuous grain boundary phase was observed with relatively large grain size. Besides, the distribution of Dy element was not uniform with obvious clusters existing in the Nd-rich phases. To regulate grain size and optimize Dy distribution, WS_2 was introduced into the Dy-containing magnets. The optimal WS_2 content in the Dy_2O_3/WS_2 co-doped magnets was 0.4 wt%. Consequently, the average grain size decreased from 8 to 6.4 μm. Relatively obvious grain boundary phase was obtained. Besides, the distribution of Dy element was more uniform due to the formation of the Nd_2O_2S phase. Therefore, the coercivity increased from 1563.2 to 1727.1 kA/m without obvious change in the remanence and the maximum energy product.

Funding Information This study was supported by the China Postdoctoral Science Foundation (No. 2018 M641188). and the Fundamental Research Funds for the Central Universities (No. FRF-TP-18-025A1).

References

1. Sawatzki, S., Kubel, C., Ener, S., Gutfleisch, O.: Grain boundary diffusion in nanocrystalline Nd-Fe-B permanent magnets with low-melting eutectics. Acta Mater. **115**, 354–363 (2016)
2. Chen, W., Luo, J.M., Guan, Y.W., Huang, Y.L., Chen, M., Hou, Y.H.: Grain boundary diffusion of Dy films prepared by magnetron sputtering for sintered Nd-Fe-B magnets. J. Phys. D. Appl. Phys. **51**, 185001 (2018)
3. Bittner, F., Woodcock, T.G., Schultz, L., Schwobel, C., Gutfleisch, O., Zickler, G.A., Fidler, J., Ustuner, K., Katter, M.: Normal and abnormal grain growth in fine-grained Nd-Fe-B sintered magnets prepared from He jet milled powders. J. Magn. Magn. Mater. **426**, 698–707 (2017)
4. Hono, K., Sepehri-Amin, H.: Strategy for high coercivity Nd-Fe-B magnets. Scripta Mater. **67**, 530–535 (2012)
5. Chen, G.X., Bao, X.Q., Lu, K.C., Lv, X.K., Ding, Y., Zhang, M., Wang, C.G., Gao, X.X.: Microstructure and magnetic properties of Nd-Fe-B sintered magnet by diffusing Pr-Cu-Al and Pr-Tb-Cu-Al alloys. J. Magn. Magn. Mater. **477**, 17–21 (2019)
6. Dan, N.H., Thanh, P.T., Yen, N.H., Huang, L.T.: Enhancing coercivity of sintered Nd-Fe-B magnets by nanoparticle addition. IEEE T. Magn. **50**, 2102204 (2014)
7. Bance, S., Fischbacher, J., Schrell, T.: Thermally activated coercivity in core-shell permanent magnets. J. Appl. Phys. **117**, 17A733 (2015)
8. Chen, F.G., Zhang, L.T., Jin, Y.X., Cheng, Y.: Simultaneous enhancement of the coercivity and remanence at high temperatures in a sintered Nd-Fe-B magnet after grain boundary diffusion with Dy60Co40 alloy. Mater. Charact. **144**, 547–553 (2018)

9. Ma, T.Y., Wang, X.J., Liu, X.L., Wu, C., Yan, M.: Coercivity enhancements of Nd-Fe-B sintered magnets by diffusing DyH_x along different axes. J. Phys. D. Appl. Phys. **48**, 2015001 (2015)
10. Kim, T.H., Lee, S.R., Kim, H.J., Lee, M.W., Jang, T.S.: Simultaneous application of Dy-X (X=F or H) powder doping and dip-coating processes to Nd-Fe-B sintered magnets. Acta Mater. **93**, 95–104 (2015)
11. Cui, X.G., Cui, C.Y., Cheng, X.N., Xu, X.J.: Effect of Dy_2O_3 intergranular addition on thermal stability and corrosion resistance of Nd-Fe-B magnets. Intermetallics. **55**, 118–122 (2014)
12. Bae, K.H., Kim, T.H., Lee, S.R., Namkung, S., Jang, T.S.: Effects of DyH_x and Dy_2O_3 powder addition on magnetic and microstructural properties of Nd-Fe-B sintered magnets. J. Appl. Phys. **112**, 093912 (2012)
13. Li, L.Y., Yi, J.H., Peng, Y.D., Huang, B.Y.: The effect of compound addition Dy_2O_3 and Sn on the structure and properties of NdFeNbB magnets. J. Magn. Magn. Mater. **308**, 80–84 (2007)
14. Ghandehari, M.H., Fidler, J.: Microstructural evidence for the magnetic surface hardening of Dy_2O_3-doped $Nd_{15}Fe_{77}B_8$ magnets. Mater. Lett. **5**, 285–288 (1987)
15. Seelam, U.M.R., Ohkubo, T., Abe, T., Hirosawa, S., Hono, K.: Faceted shell structure in grain boundary diffusion-processed sintered Nd-Fe-B magnets. J. Alloy. Compd. **617**, 884–892 (2014)
16. Gabay, A.M., Marinescu, M., Li, W.F., Liu, J.F., Hadjipanayis, G.C.: Dysprosium-saving improvement of coercivity in Nd-Fe-B sintered magnets by Dy_2S_3 additions. J. Appl. Phys. **109**, 083916 (2011)
17. Yang, F., Guo, L.C., Li, P., Zhao, X.Z., Sui, Y.L., Guo, Z.M., Gao, X.X.: Boundary structure modification and magnetic properties of Nd-Fe-B sintered magnets by co-doping with Dy_2O_3/S powders. J. Magn. Magn. Mater. **429**, 117–123 (2017)
18. Yang, F., You, L., Guo, Z.M., Paley, V., Volinsky, A.A.: Coercivity enhancement and grain refinement in Nd-Fe-B sintered magnets with pyrite doping by jet milling. J. Magn. Magn. Mater. **469**, 146–150 (2019)
19. Yang, F., Sui, Y.L., Chen, C.G., Ye, S.Y., Li, P., Guo, Z.M., Paley, V., Volinsky, A.A.: Sulfur doping effect on microstructure and magnetic properties of Nd-Fe-B sintered magnets. J. Magn. Magn. Mater. **446**, 214–220 (2018)
20. Bae, K.H., Lee, S.R., Kim, H.J., Lee, M.W., Jang, T.S.: Effect of WS_2/Al co-doping on microstructural and magnetic properties of Nd-Fe-B sintered magnets. J. Alloy. Compd. **673**, 321–326 (2016)
21. Chu, T.Y.: Evidence of domain-wall pinning in W-doped (NdDy)(FeCo)B sintered magnets. J. Appl. Phys. **76**, 6834 (1994)